LASER & PHOTONICS REVIEWS

www.lpr-journal.org

Mid-IR Supercontinuum Noise Reduction Using a Short Piece of Normal Dispersion Fiber - A General Mechanism

Rasmus Eilkær Hansen, Callum Robertson Smith, Asbjørn Moltke, Christian Rosenberg Petersen, Sidharthan Raghuraman, Seongwoo Yoo, and Ole Bang**

Mid-infrared (IR) supercontinuum (SC) lasers are important in applications such as pollution detection, stand-off detection, and non-destructive testing. The performance in many applications is limited by the noise level of the supercontinuum laser. High noise typically results in low sensitivities or a need for long integration times. In this paper, a simple technique to reduce the noise of high noise soliton-based SC sources is introduced by adding a short piece of normal dispersion fiber to force the spectrally distributed solitons to spectrally broaden through self-phase modulation and thereby overlap to average out the noise. The noise reduction is demonstrated experimentally and numerically using a ZBLAN fiber based mid-IR SC source and adding a short piece of highly nonlinear arsenic-sulfide fiber. However, the method is generally applicable to any soliton-based near-IR or mid-IR SC source. Its efficiency is underlined by experimentally comparing it to SC generation in fibers in which a second zero-dispersion wavelength provides the spectral alignment noise reduction mechanism.

1. Introduction

In the past decade, supercontinuum (SC) sources have become widely available, and found their way into many branches of analytical science and industry. Some of the most important applications include chemical sensing and imaging,[1] confocal and two-photon microscopy,[2,3] spectrally resolved photoacoustic imaging,[4] stand-off detection,[5] scanning near-field optical microscopy,[6] and spectrometer based optical coherence tomography (OCT).[7] However, the performance of these techniques is limited by the severe pulse-to-pulse fluctuations present in most SC sources. This is because traditional (such as 99% of commercial sources) SC sources use long pump pulses and are therefore based on modulational instability (MI), red-shifting solitons and soliton collisions, and the generation of optical rogue waves in the red edge of the spectrum.[8,9] These sources suffer from high relative intensity noise (RIN) due to the MI being generated from quantum noise and due to the highly phase and amplitude dependent soliton collisions. The high pulse-to-pulse noise of such MI and soliton based SC sources can be compensated by using high repetition rates to average out the noise, where the current state-of-the-art is 320 MHz.[10] Another approach is to reduce the noise on a pulse-to-pulse level. Some approaches to this include spectral alignment of solitons at a second zero dispersion wavelength (ZDW), either in the uniform fiber that generates the SC (see Figure 4) or introduced by fiber undertapering,[11] spectral alignment through gain-bands in active fibers,[12] and seeding of MI,[13] although seeding of MI is not efficient at high pump peak power.[14] These techniques offer only limited reduction of the noise (generally below a factor 4). The most efficient approach to generating low noise SC is pumping all normal dispersion (ANDi) fibers with fs laser pulses.[15,16] An ANDi SC laser can achieve noise levels an order of magnitude lower than conventional SC lasers.[17]

Unfortunately, fs lasers are comparatively expensive and do not typically provide the Watt level average powers required in many SC applications.[18] In particular, in the mid-infrared (mid-IR), the fs fiber laser technology is not so mature. Although MHz fiber lasers with 66 fs pulses have been achieved at 2 μm (Tm:SiO_2),[19] with 79 fs in a commercially available source at 2 μm,[20] and with

R. E. Hansen, C. R. Smith, A. Moltke, C. R. Petersen, O. Bang
DTU Electro
Department of Electrical and Photonics Engineering
Technical University of Denmark
Kgs. Lyngby 2800, Denmark
E-mail: raeha@fotonik.dtu.dk; oban@fotonik.dtu.dk

C. R. Petersen, O. Bang
NORBLIS APS
Virumgade 35D, Virum 2830, Denmark

S. Raghuraman, S. Yoo
School of Electrical and Electronic Engineering
The Photonics Institute
Nanyang Technological University
Singapore 639798, Singapore

S. Yoo
School of Engineering
University of Glasgow
G12 8LT Glasgow, UK

O. Bang
NKT Photonics A/S
Blokken 84, Birkerød 3460, Denmark

The ORCID identification number(s) for the author(s) of this article can be found under https://doi.org/10.1002/lpor.202200776

DOI: 10.1002/lpor.202200776

Table 1. Fiber parameters. D is the fiber diameter, NA is the numerical aperture, and n_2 is the nonlinear refractive index that we use in the numerical simulations..

Fiber	D [μm]	NA	$n_2 \times 10^{20}$ [m^2 W^{-1}]	Manufacturer
Tm/Ge:Si	12	0.28	6.0	In-house
ZBLAN A	7.5	0.26	2.1	FiberLabs Inc
ZBLAN B	6.5	0.265	2.1	FiberLabs Inc
As-S	8	0.25	420	Art photonics GmbH

180 fs at 2.8 μm (Ho:ZBLAN),[21] there has not been much work published on mid-IR normal dispersion SC generation due to the lack of suitable fibers.[22–24] The dominating SC technology in both the near-IR and mid-IR is still MI-based and thus using long pulse and high average power pump lasers. Therefore, it is important to develop simple and efficient ways of achieving noise reduction of soliton-based SC sources.

In this paper we introduce a simple technique to reduce the noise of any soliton-based SC source—both near-IR and mid-IR: Adding a short piece of normal dispersion fiber at the output to force the spectrally distributed solitons to spectrally broaden through self-phase modulation (SPM) and optical wave breaking (OWB) and thereby overlap to average out the noise. We demonstrate this noise reduction method both experimentally and numerically by adding a short piece of highly nonlinear arsenic-sulfide (As-S) fiber to a ZBLAN fiber based mid-IR SC source.

We base the demonstration on a mid-IR SC because it is an emerging technology that can cover part of the molecular fingerprint region and therefore has enormous potential in broadband spectroscopy for e.g. pollution detection[25] and food quality monitoring,[26] non-destructive testing of highly scattering materials,[27] stand-off detection,[5] all optical biopsy,[28] and bioimaging.[29] To underline the efficiency of the noise reduction mechanism we experimentally compare it to the noise reduction gained from spectral alignment at a second ZDW. We show that using the short piece of normal dispersion fiber can efficiently reduce noise over a broader bandwidth than using a second ZDW.

2. SC Source and Fiber Cascade

We consider two similar mid-IR SC sources based on SC cascading from a 1550 nm pump laser. The custom-built pump laser (Connet laser Technology, Ltd.) generates an in-amplifier SC spanning from 1500–2200 nm with a pulse duration of about 0.5 ns and 3 MHz pulse repetition rate. The spectrum is further broadened by splicing on a 30 cm Tm/Ge doped silica fiber. The Tm/Ge doped silica fiber has a core/cladding diameter of 12/125 μm and a dopant concentration of 0.15/20 wt% for Tm and Ge, respectively. The fiber was fabricated at Nanyang Technological University using an optimized chemical vapor deposition method.[30] The only difference between the two sources is the core diameter of the ZBLAN fiber used after the Tm/Ge fiber.

The parameters of the different fibers in the cascade are listed in **Table 1**, along with their manufacturer. The difference in core size of the two ZBLAN fibers (denoted ZBLAN fiber A and ZBLAN fiber B) leads to significantly different dispersion properties, as shown in **Figure 1**. Also shown is the dispersion of the highly nonlinear As-S fiber. The reduced core size of ZBLAN fiber B compared to ZBLAN fiber A leads to a second ZDW at 3.55 μm due to increased waveguide dispersion. The second ZDW stops the solitons from red-shifting further and spectrally aligns them in a wavelength region below but close to the ZDW, at which they generate and transfer energy to dispersive waves (DWs) across the ZDW, which are correspondingly spectrally aligned. A detailed comparison of the nonlinear dynamics in both cases of dispersion properties in the ZBLAN fiber is given in ref. [31]. In both cases the output of the ZBLAN fiber is coupled into a step index As-S fiber. Our calculations show that the ZDW of the As-S fiber is at 6.17 μm, which means the entire spectrum out of both ZBLAN fibers, spanning at most up to 4.5 μm, is coupled into normal dispersion. We will show that the spectrally distributed and temporally localized solitons at the long wavelength edge of ZBLAN fiber A in this way can be spectrally aligned through SPM and OWB, which will efficiently reduce the noise. In contrast, the temporally delocalized DWs in ZBLAN fiber B undergo no significant nonlinear dynamics in the As-S fiber and therefore experience no significant noise reduction.

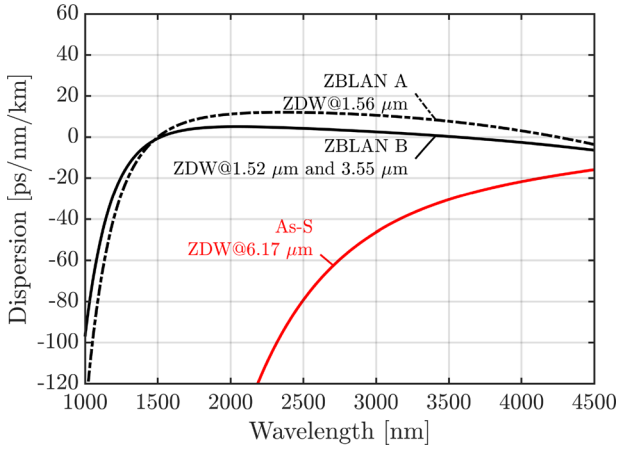

Figure 1. Dispersion profiles of ZBLAN fiber A (dashed black), ZBLAN fiber B (solid black), and the As-S fiber (solid red). The dispersion of ZBLAN fiber B is a measurement, while the dispersion of ZBLAN fiber A and the As-S fiber are calculated.

3. Experimental Section

The experimental setup is shown in **Figure 2**. The SC from the Tm/Ge fiber was free-space coupled into a ZBLAN fiber using a reflective collimator, and an anti-reflection (AR) coated (1.8–3 μm) aspheric lens with 15 and 6 mm focal length, respectively. For the ZBLAN fiber there are two options, as detailed in the figure. ZBLAN fiber A has single ZDW at 1.56 μm, and a length of 2.8 m, while ZBLAN fiber B has a second ZDW at 3.55 μm and a length of 1.05 m. In both options the output of the ZBLAN fiber was either coupled to a 0.72 m highly nonlinear As-S fiber, or directly into a monochromator. To measure the power spectral density (PSD) and the noise of the SC out of the ZBLAN fibers, the As-S fiber was not there. Coupling to the As-S fiber was achieved using a 1:1 telescope based on two 3–5 μm AR coated aspheric lenses with 6 mm focal length, and coupling to the monochromator was done with a fiber-coupled reflective

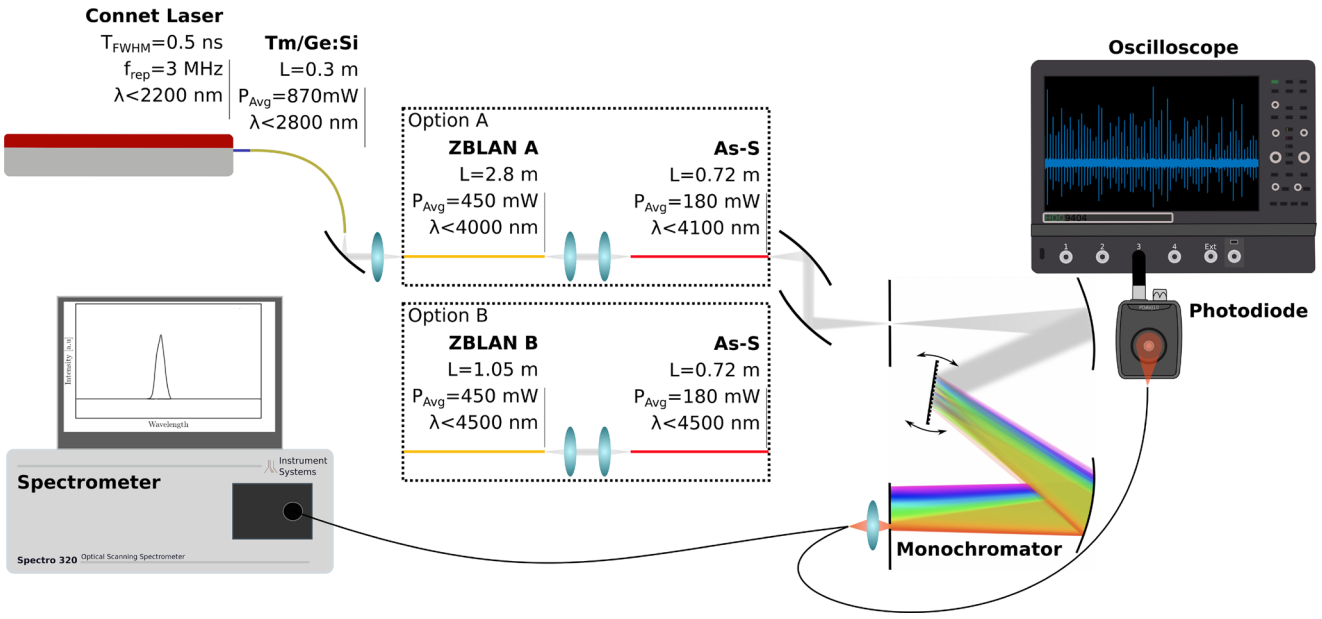

Figure 2. The experimental setup. The supercontinuum cascade is initiated by a pulsed Connet Laser module, and a Tm/Ge doped silica fiber. The remaining cascade either consists of ZBLAN fiber A or ZBLAN fiber B, followed by the As-S fiber. A Czerny–Turner type monochromator spectrally filters the light, that is subsequently measured by a photodiode, to measure the noise or a spectrometer to measure the center wavelength and spectral width at each setting on the monochromator.

collimator and a 100 mm focal length gold coated 90 degree off-axis parabolic mirror.

The monocromator was of Czerny–Turner design (Horiba iHR320). The center wavelength was controlled by rotating a diffraction grating, while the bandwidth was controlled by the exit slit size. The output of the monochromator was coupled to an InF_3 patch cable, which was either directed at a photodiode (PD) or launched into an optical spectrum analyzer (OSA) (Instrument Systems, Spectro320 covering 0.2–5μm).

The noise measurements were performed by recording a train of pulses using the fast PD and oscilloscope, as described in ref. [32]. In the following the experimental procedure is gone through, as well as the specific considerations that have been done to produce reliable noise measurements in the mid-IR.

3.1. Pulse Length and Photodiode Response Time

The noise measurements were performed with a 100 MHz MCT photodetector spanning 2–10 μm (PDAVJ10, Thorlabs, Inc.). The voltage signal from the photodiode was recorded on a 40 Gs s^{-1} oscilloscope (HDO9404, Teledyne Lecroy). The measured voltage on the photodiode operated in the linear response regime is given by

$$V_{\text{Diode-Linear}}(t) \propto \int_{-\infty}^{\infty} \text{PD}(t-t')P_{\text{Pulse}}(t')\text{d}t' \tag{1}$$

where PD(t) is the photodiode response, and P_{Pulse} is the power of the spectrally filtered optical SC pulse out of the monochromator. If the duration of P_{Pulse} is much shorter than the photodiode response time, the pulse can be considered to be a delta-function $P_{\text{Pulse}}(t') = E_P\delta(t')$, where E_{P} is the pulse energy. Using this approximation the measured voltage is

$$V_{\text{Diode-Linear}}(t) \propto E_{\text{P}}\text{PD}(t) \tag{2}$$

To use Equation (2) it must be confirmed that the spectrally filtered pulse duration can indeed be considered a delta function compared to the response time of the photodiode. As the pump pulses in the setup were ≈ 0.5 ns long, and the rise time of the photodiode was approximately $\frac{0.35}{100\ \text{MHz}} = 3.5$ ns, it was not directly evident that the pump pulses were much shorter than the photodiode response even after spectral filtering. The validity of the assumption was instead confirmed by measuring the shape of the photodiode response with a pulsed 2 μm laser that has a pulse duration of 1.9 ps (AP-TM-ML01, AdValue Photonics). As the pulses from this laser were much shorter than the rise time of the photodiode, this was considered to be a direct measurement of PD(t). In Section S3, Supporting Information, it is shown that $V_{\text{diode-Linear}}(t)$ in the noise measurements had the same shape as PD(t). Therefore, it can be argued that Equation (2) holds for the measurement of the longer SC pulses.

3.2. Photodiode Response

It was important to measure the response of the photodiode and know when it was linear and how to correct for its nonlinearity. The response was measured using the ps pulse duration 2 μm AdValue laser, by increasing the output power of the laser until saturation was reached on the photodiode. The laser light was split using a glass wedge. The photodiode response was measured in the weak reflected beam, while the average power in

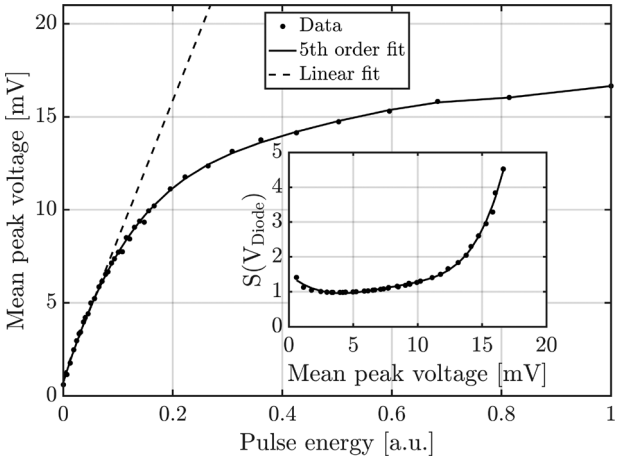

Figure 3. The measured mean peak voltage out of the photodiode as a function of the pulse energy. The response was measured with the 1.9 ps pulse duration 2 μm AdValue laser. In the inset we show the ratio of a fifth order polynomial fit to the linear fit. This scaling function $S(V_{Diode})$ is used to compensate for the nonlinearity of the photodiode response.

the transmitted beam, which was proportional to the pulse energy, was measured using a power sensor (S148C, Thorlabs, Inc.). An oscilloscope was used to measure the mean peak voltage out of the photodiode (averaged over 100 pulses) which is shown in **Figure 3** as a function of pulse energy. Ideally, the noise measurements were carried out within the linear response region (up to $\approx$ 7 mV) of the photodiode.[32] However, due to a combination of electronic noise in the photodiode (see Section S2, Supporting Information), the high laser noise, the long-tailed pulse-to-pulse distributions of the SC pulses, and the narrow linear response regime of the photodiode, this was not possible. Having measured the full nonlinear photodiode response, a correction of Equation (2) can be applied, such that the nonlinearity was taken into account. This was done by introducing a scaling function $S(V_{Diode})$, such that Equation (2) is replaced by

$$S(V_{Diode})V_{Diode} \propto E_p PD(t) \tag{3}$$

where $V_{Diode} = V_{Diode}(t)$. The scaling function $S(V_{Diode})$ is shown in the inset of Figure 3, and it is given by the ratio of the fifth order polynomial fit to the linear fit. The linear fit only used the data up to 6.6 mV. Without the scaling function the measured RIN will be severely underestimated, for instance the RIN at 3 μm was measured to be 27% at the output of ZBLAN fiber A without the scaling and 35% with the scaling. In Section S6, Supporting Information, a full comparison of the RIN is shown out of ZBLAN fiber A with and without scaling the measured voltage. In all the following figures this scaling had been applied.

3.3. Varying the Measured Power

As the SC spectra have a PSD that varies by more than an order of magnitude across the measured spectral range, a way of adjusting the incident power on the photodiode was needed. The signal was attenuated by expanding the beam size incident on the photodiode by tuning the distance between the patch cable and photodiode. This was done while maintaining the alignment, such that the center of the beam hits the center of the photodiode. In Section S1, Supporting Information, it is shown that the measured RIN values are dependent on the average voltage read-out, such that a higher voltage read-out (shorter distance between patch cable and photodiode) gave a higher measured value of the RIN. However, the change in the measured RIN when changing the average voltage read-out from 6 to 7 mV was of a similar magnitude as the variations between consecutive measurements at a constant voltage read-out (less than 0.3% in absolute values). Therefore, the distance between the patch cable and the photodiode was tuned, such that the average voltage read-out was always in the range 6–7 mV.

Each data point in the presented RIN curves was gathered in three steps:

1) Change the center wavelength on the monocromator.
2) Average 100 single pulse sweeps on the oscilloscope and ensure that the peak is in the 6–7 mV range by adjusting the distance between patch cable and photodiode.
3) Record a time trace containing 3000 pulses.

After obtaining a complete RIN curve, the patch cable was coupled into the OSA, where the filtered spectra were measured at the same monochromator settings as used in the RIN measurements. The peak wavelength in these spectra was used as the reported wavelength values while the full width half maximum (FWHM) gives the bandwidth of the measurements. The bandwidth across almost all measurements was 19 nm. However, for part of the spectrum the signal from the As-S fiber after ZBLAN fiber B was too low to measure, so instead a 38 nm bandwidth had to be used. The peak value was reported as the spectral intensity in normalized counts in **Figure 4**.

3.4. Data Analysis

Calculating the RIN curves from the obtained time traces was done in a few steps. The maximum of the pulse and the mean of the background noise floor were calculated for each pulse ($V_{Diode}(t)$). The peak value was defined as the maximum minus the floor. It was found that a universal background for an entire time trace could not be used, as there were background drifts on a longer time scale than the pulse separation. This gives an array of peak values in volts, corresponding to pulse energies on an unknown scale according to Equation (3). The peak values were scaled according to the scaling curve $S(V_{diode})$ shown in Figure 3, to compensate for the nonlinearity of the photodiode response. From the set of peak values the RIN is calculated as

$$\mathrm{RIN} = \frac{\sigma_{\text{Peak voltage}}}{\mu_{\text{Peak voltage}}} \tag{4}$$

where σ and μ are the standard deviation and mean, respectively.

4. Results

The measured PSD and RIN spectra are shown in Figure 4. Looking at the spectra we see the anticipated difference between the

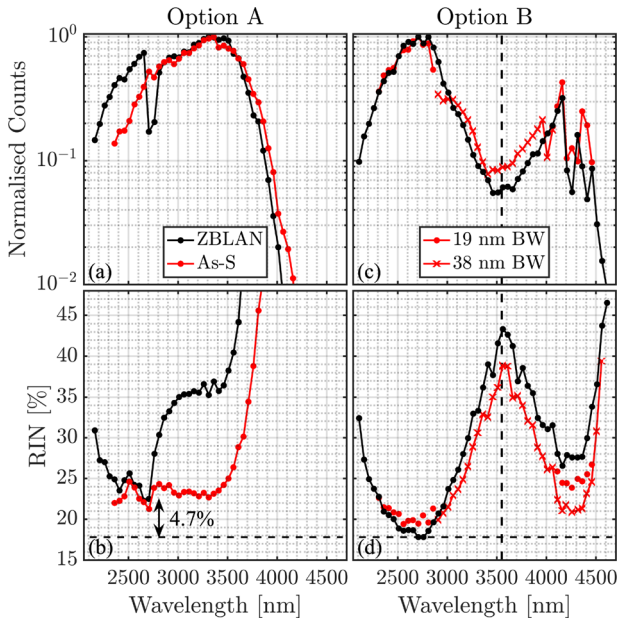

Figure 4. Measured PSD spectra in normalized counts and RIN spectral profiles. The left column shows option A, while the right column shows option B. In all cases, the black curve corresponds to the ZBLAN fiber output, while the red curves correspond to the As-S fiber output. For the dip in the spectrum out of the As-S fiber around 3.5 μm the bandwidth was 38 nm (indicated by crosses), while it was 19 nm in all other cases (indicated by dots). In option B we measured the RIN using both bandwidths in the range 4100–4500 nm to highlight the influence of the bandwidth on the measured RIN. The vertical dashed line in Option B indicates the second ZDW in ZBLAN fiber B, and the horizontal dashed lines indicate the lowest measured RIN of 17.8%. The double arrow shows the difference between the lowest RIN obtained from the two ZBLAN fibers.

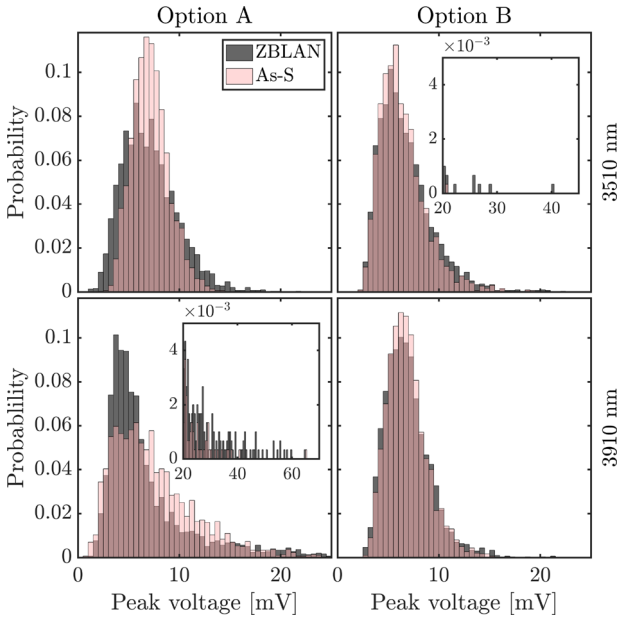

Figure 5. Histograms showing the distribution of peak voltages, corresponding to spectrally filtered pulse energies. The insets show the tail of the known L-shape in which the high energy rogue waves appear as rare events.

spectral broadening in ZBLAN fibers A and B. In both cases a large number of solitons is generated through MI.[8] Because of the smaller core diameter, the slightly higher NA, and the smaller and decreasing dispersion, the Raman redshift of the solitons is much more efficient in ZBLAN fiber B and already after less than half the length of ZBLAN fiber A, the spectrum has broadened to the loss edge. This was also demonstrated in ref. [31]. In ZBLAN fiber A we know that the whole red edge consists of solitons, whereas the second ZDW at 3.55 μm of ZBLAN fiber B makes the solitons stop before but close to 3.55 μm and very efficiently generate DWs above 3.55 μm. This gives a dip in the spectrum around 3.55 μm as seen in Figure 4c. The PSD spectrum is not shifted significantly in the As-S fiber in either case, because of its low NA and relatively large core diameter, but this was also not the intention, the intention was to demonstrate its capability of lowering the RIN.

The dynamics in ZBLAN fiber A leads to high RIN in the red edge above 2.7 μm due to solitons and rogue waves[9] (black curve in Figure 4b). The RIN in ZBLAN fiber B is much lower due to soliton and DW spectral averaging, as demonstrated in ref. [11], which is also clearly seen by comparing Figures 4b,d. At 2.8 μm the RIN is 4.7% lower in ZBLAN fiber B. The RIN out of ZBLAN fiber B becomes high in between the soliton related dip around 2.8 μm and the DW related dip around 4.2 μm simply because there is a lack of power.

When now looking at the red curves in Figure 4b–d of the RIN out of the As-S fiber, we see that the RIN is significantly lowered above 2.7 μm in ZBLAN fiber A with the soliton red edge, whereas it is only very slightly lowered in ZBLAN fiber B because its red edge above 2.8 μm already consists of spectrally aligned solitons and DWs that cannot be aligned much more. In contrast, the solitons in the red edge of ZBLAN fiber A are randomly scattered spectrally and also much more temporally scattered due to the higher purely anomalous dispersion. This effect will be demonstrated numerically in the following section.

The RIN reduction by the As-S fiber is as much as 13% for ZBLAN fiber A, from about 36% to 23%. In **Figure 5** we show a comparison between four distributions of measured peak voltages, which corresponds to pulse energies according to Equation (3). At 3510 nm the noise reduction is very efficient in option A, which is shown by a significant squeeze in the pulse energy distribution. For option B the RIN is close to 40% at 3510 nm out of both fibers, which is seen by a broad distribution left almost unchanged. In option A, 3910 nm is at the edge of the spectrum, which is also apparent in the histograms, that show a distribution with a very long tail toward high pulse energies. This L-shaped distribution at the edge of a SC spectrum is well-known to be a signature of rogue waves.[9] For option B, it is once again observed that the pulse energy distribution does not change much between the output of ZBLAN fiber B and the As-S fiber. In other words, no reduction in RIN can be achieved by spectral alignment, because the solitons and DWs are already spectrally aligned when coming out of ZBLAN fiber B.

4.1. Numerical Results

In the following we support our experimental conclusions with numerical modeling and provide further insight into the soliton

and DW spectral alignment effect. All SC simulations have been carried out with the generalized nonlinear Schrödinger equation solver described in ref. [33]. Since our aim is to demonstrate the qualitative effect, we consider a scalar model with only the fundamental mode. The model includes the full dispersion curve, such that no Taylor expansion of β_2 was necessary. Furthermore, mode profile dispersion (frequency dependence of the effective area) as described in ref. [34] was included. The ZBLAN and As-S loss curves are from measurements of fibers of the same material. All fiber parameters used in the simulations, including how/where they have been obtained, are given in Section S4, Supporting Information. A temporal resolution of 1.5 fs, and 2^{19} grid points was used in all simulations. All presented results are an average of 50 simulations with one-photon-per-mode quantum noise, and 1% RIN of the pump laser.[35] The model was implemented in C and parallelized in the stepper using OpenMP. The computations were performed on a high performance cluster using 300 computing cores. A running average with a bandwidth of 19 nm was applied to the PSD before finding the standard deviation and mean, such that the filter bandwidth matches the experiment.

To numerically demonstrate the effect of noise reduction we first need the SC that is pumping the ZBLAN fibers. A representative soliton-based SC with a red edge around the experimentally observed 2.6 μm is sufficient for a qualitative demonstration. We generate this representative spectrum using a 2.5 m long SMF-28 fiber with an increased nonlinear refractive index of $n_2 = 6 \times 10^{20}$ m^2 W^{-1}. The SMF-28 fiber is pumped with 25 ps (FWHM in intensity), 15 kW peak power pulses (Gaussian shaped) from a 1550 nm laser, with the repetition rate of the real pump laser (3 MHz) this corresponds to 1.06 W average power. For the ZBLAN SC generation we used a 10 m long ZBLAN fiber A and a 2 m long ZBLAN fiber B. These lengths were chosen to reproduce the experimentally observed IR edge in ZBLAN fiber A and the strength of the DW peak in ZBLAN fiber B. The simulated length of the As-S fiber was 20 cm because this was sufficient to see the full noise reduction. A coupling efficiency of 40% was assumed between the ZBLAN fibers and the As-S fiber. The numerical results, corresponding to the experimental results in Figure 4 are shown in **Figure 6**. Qualitatively, there is good agreement in that there is extreme noise reduction in option A, while the noise reduction is limited in option B. In the spectra, many of the features match those from the experimental measurements, including the presence of the second ZDW in option B that creates DWs, and a dip in the spectrum close to the ZDW at 3.55 μm. The short propagation in the As-S fiber is seen to have no influence on the DWs at 4.2–4.3 μm as these are not temporally localized. In option A the spectrum out of the ZBLAN fiber extends almost to 4 μm, as is the case in the experiments. However, there are also a few discrepancies. In the measured ZBLAN spectrum in option A there is a dip around 2700 nm, which is a measurement artifact from one of the optical density filters in our OSA. In the experimental spectra in option B there are also two dips in the spectra at 4200–4300 nm. These dips are due to CO_2 absorption in the free space beam paths of the experimental setup. The spectral broadening in the As-S fiber in option A is much more efficient than in the experiments, therefore the noise reduction is also more significant in the simulations.

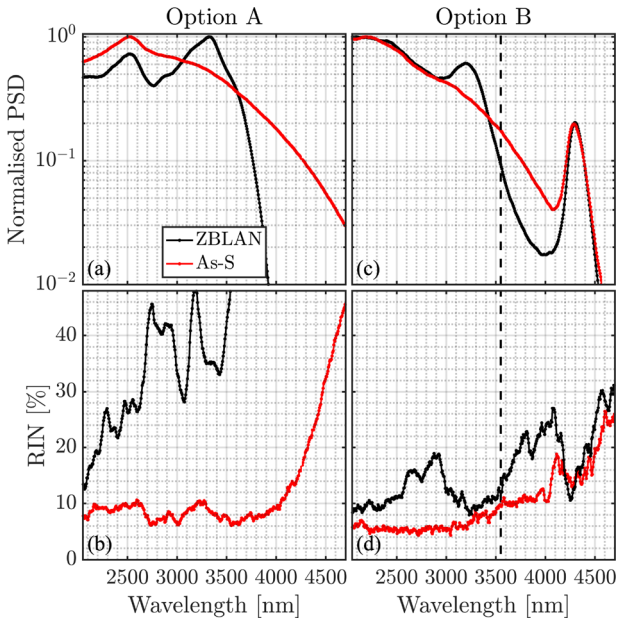

Figure 6. Simulated PSD spectra and RIN profiles. The left column shows option A, while the right column shows option B. In all cases a black curve is the RIN out of a ZBLAN fiber, while the red curves are out of the As-S fiber. The dashed line in Option B indicates the second ZDW in the ZBLAN fiber.

The simulations confirm the experimentally observed significant noise reduction in the soliton rich case (option A), while the noise reduction in option B is very limited. In fact, the extreme noise reduction in the simulations is encouraging for further optimization of the SC cascade. Better correspondence between experiments and simulations could be achieved by changing some of the simulated fiber parameters, such as the nonlinear refractive index, which is not known with certainty. The primary limitations of the simulations is that the exact dispersion of all fibers have not been measured, and that the simulations do not consider the active Er and Tm/Ge doped silica fibers. However, exact correspondence between simulations and measured results is not the purpose of the simulations. Instead, the purpose is to illustrate the origin of the noise reduction, as shown in the spectrogram series in **Figure 7**.

In the left column of Figure 7, a single shot of the pulse propagation in the As-S fiber when pumped by ZBLAN fiber A is shown. The input consists mainly of temporally and spectrally distributed pulses. After just 10 cm of propagation, the pulses have spectrally broadened such that there is a significant spectral overlap between individual pulses. The broadening happens independently for each pulse, and in ref. [33] we demonstrated through simulations that the broadening is due to SPM and OWB of each pulse. In that work we also showed how one can generate so-called SPM rogue waves when many of the SPM and OWB broadened pulses are sufficiently close together spectrally (within the Raman gain bandwidth) to allow one pulse to swallow the energy of all the others. The subsequent 10 cm of propagation shows no significant broadening. This suggests that the noise reduction happens almost immediately, and that the length of the As-S fiber could be chosen as short as a few tens of cm, or what

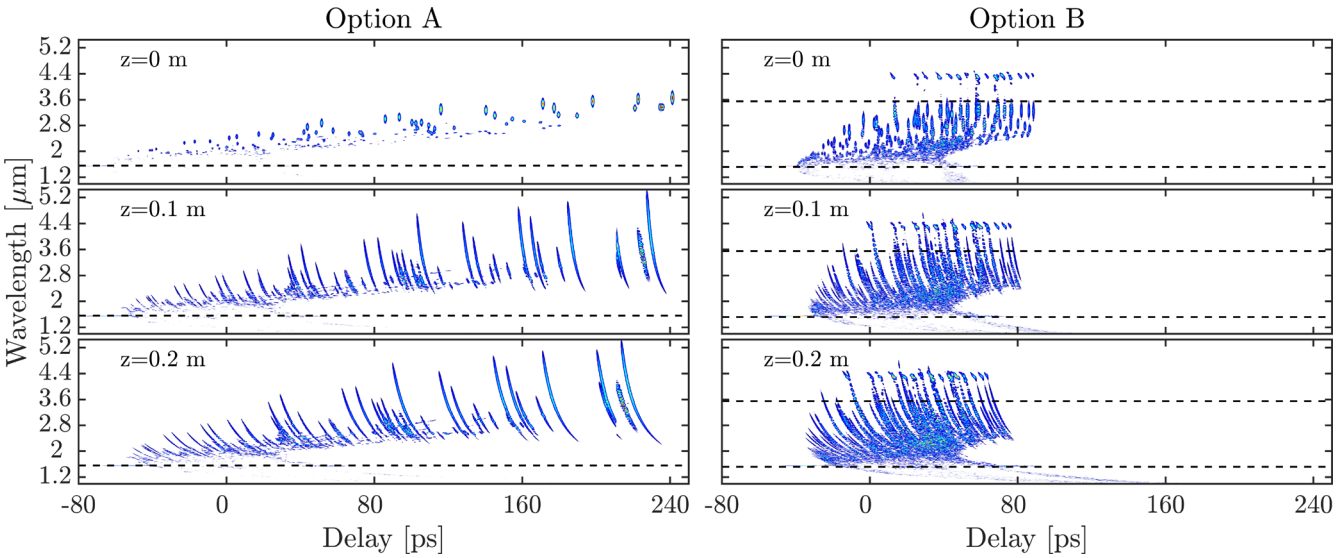

Figure 7. Spectrogram series of the dynamics in the As-S fiber when the input comes from ZBLAN fiber A (left column) and ZBLAN fiber B (right column). All spectrograms are made with a window width of 0.5 ps, and the color scales are normalized to the maximum of each spectrogram. The dashed lines indicate the ZDWs in the corresponding ZBLAN fibers.

can practically be handled. In the right column, the propagation in the As-S fiber when pumped by ZBLAN fiber B is shown. As ZBLAN fiber B is much shorter than ZBLAN fiber A (2 m vs 10 m in the simulations), and because the magnitude of the dispersion is lower, the light is more temporally localized. The input spectrum shows the remnants of a lot of spectrally aligned solitons, that have each generated a DW across the ZDW. Each DW remains relatively unaffected by propagating in the As-S fiber, which again confirms the experimental observation that the noise is not lowered significantly, simply because the solitons and DWs are already spectrally aligned.

We have focused on the RIN which, for spectrometer based applications, is the most useful noise measure. However, the phase coherence is often reported in the literature along with the RIN.[16,18,36] Coherence is a measure of phase stability from pulse to pulse. Our simulations show that the significant reduction in RIN does not lead to an improvement in coherence. The coherence was calculated using the definition given in ref. [37], omitting the integral over frequency to maintain a spectrally dependent measure. For a full analysis of the simulated spectral and RIN evolution in all fibers, see Section S5, Supporting Information.

5. Conclusion

There are three parts to the findings of this paper. One is of a general nature: We have experimentally and numerically shown that the noisy output of an MI and soliton based SC laser can be greatly reduced through spectral alignment from SPM and OWB by coupling the light into a short piece of fiber with normal dispersion.

The second finding is specifically related to noise in cascaded mid-IR SC generation. We have shown both experimentally and numerically how coupling a soliton based SC into normal dispersion in a highly nonlinear As-S fiber leads to significant noise reduction. Numerical simulations confirm that this is due to rapid spectral broadening of each soliton through SPM and OWB, which leads to spectral alignment. In a broad window from 2700 nm to 3500 nm the RIN is reduced from ≈36% to ≈ 23%. This is a significant reduction that would for example directly impact the image quality in OCT, resulting in clearer features and reduced speckle.[38] The simulations suggest that more efficient spectral broadening in the As-S fiber would lead to an even more significant noise reduction.

Finally, for the first time we experimentally and numerically compared the performance of two methods of achieving noise reduction: A) Using soliton spectral alignment by adding a piece of normal dispersion fiber and B) by generating the SC in a fiber with a second ZDW. This has revealed that using a section of normal dispersion fiber (ZBLAN fiber A + As-S fiber) is generally more efficient than using a second ZDW (ZBLAN fiber B). This is because of the broad spectral region around the second ZDW having a very low PSD and therefore high RIN. In a narrow region close to but sufficiently far from the second ZDW method (B) gives lower noise than method (A). We further show that method (B) cannot be used to significantly reduce the noise achieved with method (A).

Supporting Information

Supporting Information is available from the Wiley Online Library or from the author.

Acknowledgements

The authors thank VILLUM FONDEN(2021 Villum Investigator project no. 00037822: Table-Top Synchrotrons), EU H2020-ICT-37 (TRIAGE project, 101015825), Innovation Fund Denmark through UVSUPER Grant No. 8090-00060A, EU Horizon-CL4-2021-TWIN-TRANSITION-01 (ZDZW project, 101057404), and EU Horizon-CL4-2021-TWIN-TRANSITION-01 (TURBO project, 101058054).

Conflict of Interest

The authors declare no conflict of interest.

Data Availability Statement

The data that support the findings of this study are available from the corresponding author upon reasonable request.

Keywords

chalcogenide glass fibers, self-phase modulation, solitons, supercontinuum generation, supercontinuum noise reduction, ZBLAN fibers

Received: October 13, 2022
Revised: February 22, 2023
Published online: April 9, 2023

[1] C. F. Kaminski, R. S. Watt, A. D. Elder, J. H. Frank, J. Hult, *Appl. Phys. B* **2008**, *92*, 367.
[2] K. Shi, P. Li, S. Yin, Z. Liu, *Opt. Express* **2004**, *12*, 2096.
[3] R. T. Borlinghaus, *The White Confocal*, Springer, Cham **2017**.
[4] M. K. Dasa, C. Markos, M. Maria, C. R. Petersen, P. M. Moselund, O. Bang, *Biomed. Opt. Express* **2018**, *9*, 1762.
[5] M. Kumar, M. N. Islam, F. L. Terry, M. J. Freeman, A. Chan, M. Neelakandan, T. Manzur, *Appl. Opt.* **2012**, *51*, 2794.
[6] K. J. Kaltenecker, S. Rao D. S., M. Rasmussen, H. B. Lassen, E. J. R. Kelleher, E. Krauss, B. Hecht, N. A. Mortensen, L. Grüner-Nielsen, C. Markos, O. Bang, N. Stenger, P. U. Jepsen, *APL Photonics* **2021**, *6*, 066106.
[7] I. Hartl, X. D. Li, C. Chudoba, R. K. Ghanta, T. H. Ko, J. G. Fujimoto, J. K. Ranka, R. S. Windeler, *Opt. Lett.* **2001**, *26*, 608.
[8] J. M. Dudley, G. Genty, S. Coen, *Rev. Mod. Phys.* **2006**, *78*, 1135.
[9] D. R. Solli, C. Ropers, P. Koonath, B. Jalali, *Nature* **2007**, *450*, 1054.
[10] M. Maria, I. B. Gonzalo, T. Feuchter, M. Denninger, P. M. Moselund, L. Leick, O. Bang, A. Podoleanu, *Opt. Lett.* **2017**, *42*, 4744.
[11] R. D. Engelsholm, O. Bang, *Opt. Express* **2019**, *27*, 10320.
[12] K. Kwarkye, M. Jensen, R. D. Engelsholm, M. K. Dasa, D. Jain, P. Bowen, P. M. Moselund, C. R. Petersen, O. Bang, *Sci. Rep.* **2020**, *10*, 8230.
[13] D. R. Solli, C. Ropers, B. Jalali, *Phys. Rev. Lett.* **2008**, *101*, 233902.
[14] S. T. Sørensen, C. Larsen, U. Møller, P. M. Moselund, C. L. Thomsen, O. Bang, *J. Opt. Soc. Am. B* **2012**, *29*, 2875.
[15] C. Finot, B. Kibler, L. Provost, S. Wabnitz, *J. Opt. Soc. Am. B* **2008**, *25*, 1938.
[16] A. M. Heidt, A. Hartung, G. W. Bosman, P. Krok, E. G. Rohwer, H. Schwoerer, H. Bartelt, *Opt. Express* **2011**, *19*, 3775.
[17] E. Genier, S. Grelet, R. D. Engelsholm, P. Bowen, P. M. Moselund, O. Bang, J. M. Dudley, T. Sylvestre, *Opt. Lett.* **2021**, *46*, 1820.
[18] T. Sylvestre, E. Genier, A. N. Ghosh, P. Bowen, G. Genty, J. Troles, A. Mussot, A. C. Peacock, M. Klimczak, A. M. Heidt, J. C. Travers, O. Bang, J. M. Dudley, *J. Opt. Soc. Am. B* **2021**, *38*, F90.
[19] A. M. Heidt, J. Modupeh Hodasi, A. Rampur, D.-M. Spangenberg, M. Ryser, M. Klimczak, T. Feurer, *Sci. Rep.* **2020**, *10*, 16734.
[20] https://www.thorlabs.com/newgrouppage9.cfm?objectgroup_ID=8652 (accessed: Sept 2022).
[21] S. Antipov, D. D. Hudson, A. Fuerbach, S. D. Jackson, *Optica* **2016**, *3*, 1373.
[22] T. S. Saini, T. H. Tuan, T. Suzuki, Y. Ohishi, *Sci. Rep.* **2020**, *10*, 2236.
[23] S. Kedenburg, T. Steinle, F. Mörz, A. Steinmann, H. Giessen, *Opt. Lett.* **2015**, *40*, 2668.
[24] B. Kibler, A. Lemière, J.-T. Gomes, D. Gaponov, L. Lavoute, F. Désévédavy, F. Smektala, *Opt. Commun.* **2021**, *488*, 126853.
[25] M. A. Abbas, K. E. Jahromi, M. Nematollahi, R. Krebbers, N. Liu, G. Woyessa, O. Bang, L. Huot, F. J. M. Harren, A. Khodabakhsh, *Opt. Express* **2021**, *29*, 22315.
[26] K. Eslami Jahromi, Q. Pan, A. Khodabakhsh, C. Sikkens, P. Assman, S. M. Cristescu, P. M. Moselund, M. Janssens, B. E. Verlinden, F. J. M. Harren, *Sensors* **2019**, *19*, 10.
[27] N. M. Israelsen, C. R. Petersen, A. Barh, D. Jain, M. Jensen, G. Hannesschläger, P. Tidemand-Lichtenberg, C. Pedersen, A. Podoleanu, O. Bang, *Light: Sci. Appl.* **2019**, *8*, 11.
[28] A. Seddon, B. Napier, I. Lindsay, S. Lamrini, P. Moselund, N. Stone, O. Bang, *Laser Focus World* **2016**, *52*, 50.
[29] C. R. Petersen, N. Prtljaga, M. Farries, J. Ward, B. Napier, G. R. Lloyd, J. Nallala, N. Stone, O. Bang, *Opt. Lett.* **2018**, *43*, 999.
[30] S. Chen, Y. Jung, S. Alam, D. J. Richardson, R. Sidharthan, D. Ho, S. Yoo, J. M. O. Daniel, *Opt. Express* **2019**, *27*, 36699.
[31] C. R. Petersen, P. M. Moselund, C. Petersen, U. Møller, O. Bang, *Opt. Express* **2016**, *24*, 749.
[32] C. R. Smith, R. D. Engelsholm, O. Bang, *Opt. Express* **2022**, *30*, 8136.
[33] R. E. Hansen, R. D. Engelsholm, C. R. Petersen, O. Bang, *J. Opt. Soc. Am. B* **2021**, *38*, 2754.
[34] J. Lægsgaard, *Opt. Express* **2007**, *15*, 16110.
[35] E. Genier, P. Bowen, T. Sylvestre, J. M. Dudley, P. Moselund, O. Bang, *J. Opt. Soc. Am. B* **2019**, *36*, A161.
[36] J. M. Dudley, G. Genty, S. Coen, *Rev. Mod. Phys.* **2006**, *78*, 1135.
[37] J. Lægsgaard, *Opt. Lett.* **2018**, *43*, 2744.
[38] D. S. S. Rao, M. Jensen, L. Grüner-Nielsen, J. Olsen, P. Heiduschka, B. Kemper, J. Schnekenburger, M. Glud, M. Mogensen, N. Israelsen, O. Bang, *Light: Sci. Appl.* **2021**, *10*, 1333.